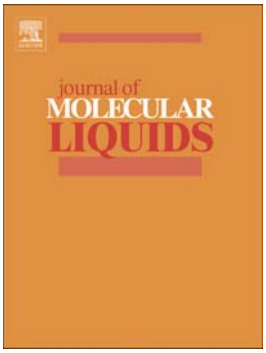

Spectroscopic and molecular structure characterization of Cu(II), Co(II), Ni(II) and Fe (III) amoxicillin antibiotic drug complexes in alcoholic media

M.A. Hussien, Samy M. El-Megharbel, Moamen S. Refat

PII: S0167-7322(16)30449-4
DOI: doi: 10.1016/j.molliq.2016.05.050
Reference: MOLLIQ 5864

To appear in: *Journal of Molecular Liquids*

Received date: 22 February 2016
Revised date: 3 May 2016
Accepted date: 18 May 2016

Please cite this article as: M.A. Hussien, Samy M. El-Megharbel, Moamen S. Refat, Spectroscopic and molecular structure characterization of Cu(II), Co(II), Ni(II) and Fe (III) amoxicillin antibiotic drug complexes in alcoholic media, *Journal of Molecular Liquids* (2016), doi: 10.1016/j.molliq.2016.05.050

Spectroscopic and molecular structure characterization of Cu(II), Co(II), Ni(II) and Fe (III) amoxicillin antibiotic drug complexes in alcoholic media

M.A. Hussien[1], Samy M. El-Megharbel [2, 3*] and Moamen S. Refat [1, 2]

[1]*Department of Chemistry, Faculty of Science, Port Said University, Port Said, Egypt*

[2]*Department of Chemistry, Faculty of Science, Taif University, Al-Hawiah, Taif, P.O. Box 888 Zip Code 21974, Saudi Arabia*

[3]*Department of Chemistry, Faculty of Science, Zagazig University, Zagazig 44519,*

**Corresponding author: Dr. Samy M. El-Megharbel*

E-mail address: samyelmegharbel@yahoo.com

Abstract

Herein, this paper aimed to preparation, molecular structure characterizations, spectroscopic and thermal studies of Cu(II), Co(II), Ni(II) and Fe(III) chelates of amoxicillin (AMX) antibiotic drug. The stoichiometry of 1:2 (Metal : AMX) complexes were explained by micro–analytical analyses and spectroscopic tools (e.g., FT–IR, ESR and UV–vis.). The values of molar conductance for the AMX complexes dissolved in dimethylsulfoxide led to electrolytic behavior. These outcome data prove that AMX acts with mentioned metal chlorides as a tri–dentate chelate through $–NH_2$, –NH, and oxygen of carbonyl *β*-lactam groups. The general formula of AMX complexes can be summarized as $[M(AMX\text{-}Na)_2].xCl.yH_2O$ (where M= Cu^{2+} (*x*= 2, *y*= 4), Co^{2+} (*x*= 2, *y*= 2), Ni^{2+} (*x*= 2, *y*= 1) and Fe^{3+} (*x*= 3, *y*= 0). The activation thermodynamic parameters E*, ΔS*, ΔH* and ΔG* were estimated using two official methods as Coats–Redfern and Horowitz–Metzger dependent on thermogravimetric curves. The molecular structure of AMX drug was optimized by HF method with 3-21G basis. The molecular docking analysis was carried out using the receptor of prostate cancer mutant 2Q7K–hormone.

Key words: Amoxicillin, spectroscopic, complexation, thermal, 2Q7K–hormone.

1- Introduction

The trend of metal–drug complexes as bioinorganic branch has been received a great attention compared with free drugs [1-6]. The metal–drug binding led to drastic changes in the pharmaceutical properties of drugs [3, 5]. The type of metal ions was an essential backbone in the metallo (antibiotic skeletons, that made to modify the medical efficiency [7-10]. Antibiotics metal complexes were found more therapeutic effective rather than their mentioned antibiotics [8-10]. The literature survey revealed greater attention for the important roles of metal chelates as antitumor activities [11, 12]. The transfer of metal ion from the ligand to the viruses associated with cancer is a mechanism for releasing the anticancer drug in the locality of the tumor [12].

The biosynthesis of biocompatible gold nanoparticles (GNPs) from an aqueous extract of the aerial parts of a pteridophyte, "Adiantum philippense" by microwave irradiation and its surface functionalization with broad spectrum beta lactam antibiotic, amoxicillin (Amox) has been discussed [13], The functionalization of amoxicillin on GNPs (GNP-Amox) was carried out via electrostatic interaction of protonated amino group and thioether moiety mediated attractive forces.

Different chemometric models were applied for the quantitative analysis of amoxicillin (AMX), and flucloxacillin (FLX) in their binary mixtures [14], namely, partial least squares (PLS), spectral residual augmented classical least squares (SRACLS), concentration residual augmented classical least squares (CRACLS) and

artificial neural networks (ANNs). All methods were applied with and without variable selection procedure (genetic algorithm GA). The methods were used for the quantitative analysis of the drugs in laboratory prepared mixtures and real market sample via handling the UV spectral data. Robust and simpler models were obtained by applying GA. The proposed methods were found to be rapid, simple and required no preliminary separation steps.

Amoxicillin is (Fig. 1) an analog of ampicillin, derived from the basic penicillin nucleus [13-15]. Amoxicillin is a member of penicillin's group which is a very important class of β–lactamic antibiotics used in therapy because of its specific toxicity towards bacteria. From a coordination chemistry perspective, it has been demonstrated that all the β–lactamic antibiotics possess a number of potential donor sites and they are known to interact effectively with several metal ions and organometallic moieties [16, 17]. Atoms involved in coordination and the structure of these complexes depend on several factors, including reaction medium, pH, conformational equilibrium occurring in solution state and the nature of the side chain bonded of the β–lactamic ring. The β–lactam antibiotics possess a number of potential donor sites, which interact effectively with Lewis acidic metals [18, 19]. The stereochemistry and geometries of such complexes are highly dependent on several factors, including the reaction medium, pH and the nature of the side chain bonded to the phenyl of the β–lactam ring. The pharmacology, clinical efficiency, resistance with enzymes to β–lactam antibiotics and coordination chemistry with amoxicillin has been reported [20-22].

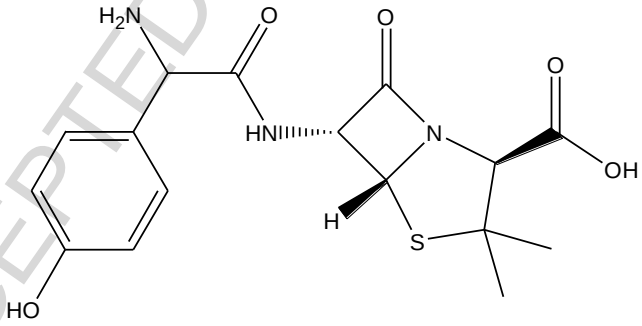

Fig. 1: The amoxicillin antibiotic drug (AMX)

Amoxicillin trihydrate and ampicillin trihydrate have been coordinated to copper salts in a 1:1 molar ratio in the presence of biuret reagent to form mixed ligand copper complexes [23], which were further used for the treatment of the infections caused by most of the Gram positive and Gram negative bacteria [24]. Their protein synthesis-inhibiting properties [25] due to their acidic nature were also reported [26]. The basic nucleus of the antibiotics is 6–amino penicillanic acid, which consists of a thiolidine ring linked to a β–lactam ring with a side chain [27, 28]. Many studies concerning the biochemical and pharmaceutical effects of antibiotics when complexed with metal ions have been a subject of great interest for many scientists. Amoxicillin antibiotic, known as 6–[D–α–(p-hydroxyphenyl) acetamido] pencilanic acid, has effect against urinary tract infection and used in the treatment of respiratory infections and meningitis [29]. The metal complexation behavior of amoxicillin was studied extensively. Lyle and Yassin [30] studied the differential pulse polarographic behaviour of nickel (II) complex with amoxicillin at the dropping mercury electrode. Novel di and tri organotin (IV) derivatives of amoxicillin of the type $R_2SnCl(Amox).2H_2O$, $R_2Sn(Amox)_2.2H_2O$ and $R_3SnCl(AmoxH)Na.2H_2O$ (R = Me, Bu and Ph) had been reported [31], these studies suggested that amoxicillin in the diorgano derivatives behaved

as monoanionic (Amox = deprotonated amoxicillin) bidentate ligand, coordinating the tin (IV) ion through the ester type carboxylate and lactamic carbonyl. However in the triorgano derivative, $R_3SnCl(AmoxH)Na.2H_2O$, the tin is coordinated only through the lactamic carbonyl that acts as monodentate ligand. In both $R_2SnCl(Amox)2H_2O$ and $R_3SnCl(AmoxH)Na.2H_2O$ trigonal bipyramidal configuration were proposed while in $R_2Sn(Amox)_2.2H_2O$ the coordination geometry at Sn(IV) was skew–trapezoidal bipyramid, with two chelating amoxicillin acted as bidentate ligand in the trapezoidal plane and the organic molecules in axial positions. Novel triorganotin(IV) complexes of two β–lactamic antibiotics, 6-[d-(−)–β–amino–p–hydroxyphenyl–acetamido] penicillin and 6-[d-(−)-α-aminobenzyl]penicillin, have been synthesized and investigated both in solid and solution states. These complexes corresponded to the general formula $R_3Sn(IV)antib{\cdot}H_2O$ (R=Me, n-Bu, Ph; antib=amox=amoxicillinate or amp=ampicillinate) [32]. Amoxicillin acted as monoanionic bidentate ligand coordinating the metal ion through carboxylate as well as through the lactamic carbonyl group in its complexes with some transition metal ions; Ag(I), Cu(II), Co(II), Zn(II) and Ni(II) [33]. To know whether the amoxicillin act as ionic or in neutral manner on coordination, The synthesis and characterization of heterobinuclear complexes of the general formula $[MCl_3(AmoxH)MCl_2]$ (where M = titanium (III), chromium (III) and iron (III); M = zinc (II) and cadmium (II); AmoxH = amoxicillin) were described [34] and amoxicillin exhibited penta-dentate manner. The three sites along with the three chloride ions were used to form the most probable octahedral geometry around the trivalent metal ions Ti(III), Cr(III) and Fe(III), while the other two sites with the two other chloride ions were utilized to form the most probable tetrahedral arrangement around the divalent metal ions Zn(II) and Cd(II). Complexes of amoxicillin with Bi(V) were obtained in acidic media [35]. The new complexes of amoxicillin with some transition metal ions such as Ag(I), Cu(II), Co(II), Zn(lI) and Ni(II) showed an enhanced antibacterial activity against several *Escherichia coli, Staphylococcus aurous, Pseudonomous aerugionosa* compared to the simple antibiotic [33]. Metal such as Co (II), Ni (II), Cu (II) and Bi (V) were coordinated to a novel ligand which was made by coupling gentamicin and amoxicillin. These were studied by various spectroscopic techniques which indicated a square planar arrangement of ligand around the Co(II) ions [36]. Also, complexes of Co(II), Zn(II), Ni(II) and Mn(II) with cinnemaldehyde , p–chlorobenzaldehyde and amoxicillin trihydrate were synthesis and characterized [37]. The interaction of amoxicillin with Zn (II) ion has been found to form one complex of 1:1 metal to ligand composition. The results showed that the complex formation was affected by the nature of solvents, time, pH and temperature [38]. The interaction of Al(III) with amoxicillin (L) was studied by the pH-metric titration in aqueous solutions at 20 °C and ionic strength 0.1 (KNO_3). In weakly acidic medium, complexes with the composition Al(OH)L and $Al(OH)_2L$ were formed [39].

In continuation of our work in the branch of metal–drug interactions [40-45], this study aimed to synthesis, theoretical calculations, spectroscopic characterizations, thermal stabilities and their molecular docking calculation of amoxicillin antibiotic drug complexes of Cu(II), Co(II), Ni(II) and Fe(III) ions in alcoholic media. The experimental studies have been matched with suggested structures.

2- Experimental

2-1- Materials

Amoxicillin trihydrate antibiotic drug was received from the Aldrich chemical company. All of chemicals used in this study were of analytically reagent grade, commercially available from BDH and used without previous purification like $CuCl_2$, $CoCl_2$, $NiCl_2$ and $FeCl_3$ salts.

2-2- Preparations

The copper(II), cobalt(II), nickel(II) and iron(III) amoxicillin complexes were synthesized similarly according to the following procedure: 2 mmol of amoxicillin trihydrate ligand was dissolved in 20 mL methanol then mixed with 20 mL of methanolic solution of 1 mmol of each metal salts $CuCl_2$, $CoCl_2$, $NiCl_2$ and $FeCl_3$. A mixture of 1:2 ratio (metal ions: AMX) at pH 7–8 (adjusted by adding 1 M a methanolic sodium hydroxide solution) was heated under reflux and continuous stirring at 50–60 ^oC for about 4 hrs. The mixtures were remaining overnight at room temperature until precipitation settled down. The colored precipitates were filtered off and washed three times using methanol solvent. The solid products were dried under vacuum over anhydrous $CaCl_2$. The yield percent of the products collected were about 72–89%.

2-3-Instruments

The micro−analytical analyses of %C, %H and %N percentages were calculated using a Perkin Elmer CHN 2400 (USA). The molar conductivities of AMX complexes with 10^{-3} mol/cm^3 concentration in DMSO solvent were measured by Jenway 4010 conductivity meter. The UV-vis absorption spectra were recorded in DMSO solvent within 800-200 nm range using a UV2 Unicam UV/Vis Spectrophotometer fitted with a quartz cell of 1.0 cm path length. The infrared spectra with KBr discs were recorded on Bruker FT-IR Spectrophotometer (4000–400 cm^{-1}). Magnetic moments were calculated using the Magnetic Susceptibility Balance, Sherwood Scientific, Cambridge Science Park, Cambridge, England, at Temp 25 ^oC. The thermal studies TG/DTG–50H were carried out on a Shimadzu thermo gravimetric analyzer under nitrogen till 800 ^oC. ESR measurements of powdered samples were recorded at room temperature using an X-band spectrometer utilizing a 100 kHz Magnetic Field Modulation with diphenyl picrylhydrazyle (DPPH) as a reference sample.

3- Results and Discussion

3-1- Analytical and physical data

The formulas and physicochemical behavior of the AMX antibiotic drug with $CuCl_2$, $CoCl_2$, $NiCl_2$ and $FeCl_3$ salts are listed in Table 1. The AMX solid compounds are stable at room temperature with higher melting points. The binding of AMX drug towards mentioned metal ions was assigned based on FT−IR, UV−vis., ESR, magnetic analyses as well as thermal analyses and molar conductance. The ratio of %carbon, %hydrogen, %nitrogen, %chloride and %metal ions in experimental work are in agreement with the theoretical data. These data led to 1:2 (metal:AMX) stoichiometry for all complexes. The electrolytic behavior [46] of the AMX complexes are due the presence of chloride ions in ionic form outside the chelation sphere. The effective magnetic moment of paramagnetic complexes of AMX was calculated at room temperature. The results are matched with the speculated formulas; $[M(AMX\text{-}Na)_2].xCl.yH_2O$ (where M= Cu^{2+} (x= 2, y= 4) complex **1**, Co^{2+} (x= 2, y= 2) complex **2**, Ni^{2+} (x= 2, y= 1) complex **3**, and Fe^{3+} (x= 3, y= 0) complex **4** (Fig. 2).

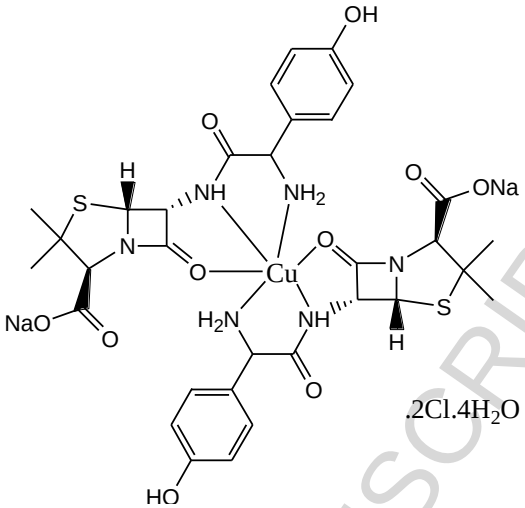

.2Cl.4H_2O

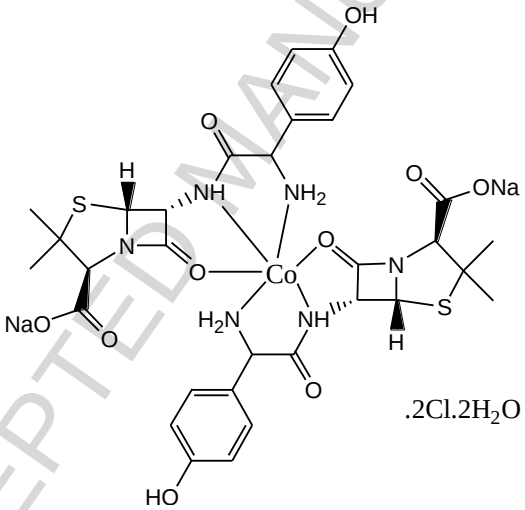

.2Cl.2H_2O

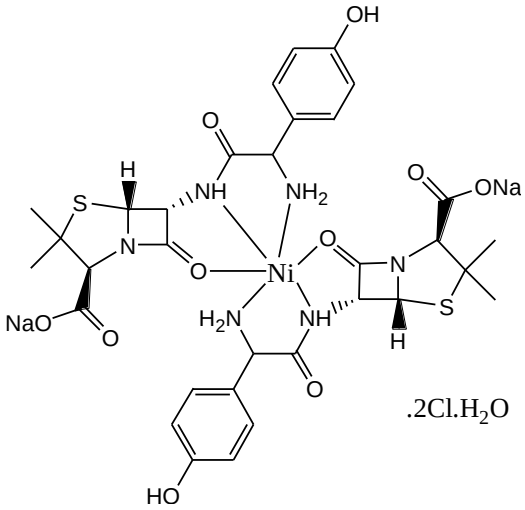

.2Cl.H_2O

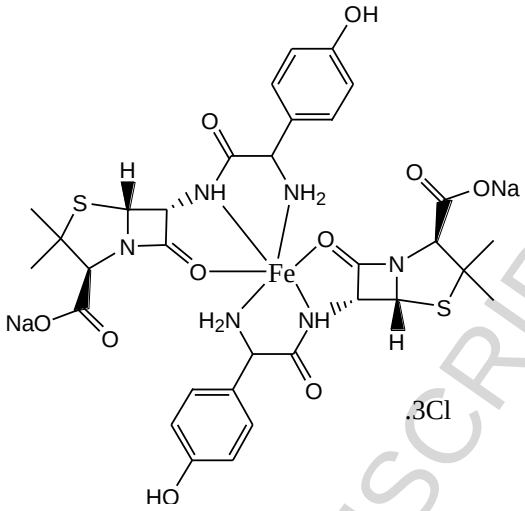

Fig. 2: Speculated formulas of complexes **1**–**4**

Table1: Micro−analytical and physical data of AMX drug and their metal complexes

Compounds	Color	M.P/^{o}C	Λm (μS)	Elemental analysis, % Found % (Calcd.)				
				C	H	N	Cl	M
AMX	White	>200	12	52.59	5.24	11.50	-	-
Complex **1**	Green	>250	116	39.17 (39.14)	4.52 (4.33)	8.56 (8.45)	7.23 (7.18)	6.48 (6.41)
Complex **2**	Red	>250	104	40.86 (40.80)	4.29 (4.24)	8.93 (8.90)	7.54 (7.41)	6.27 (6.22)
Complex **3**	Green	>250	98	41.67 (41.54)	4.15 (4.09)	9.11 (9.06)	7.69 (7.62)	6.36 (6.30)
Complex **4**	Dark brown	>250	186	41.02 (40.97)	3.87 (3.82)	8.97 (8.90)	11.35 (11.24)	5.96 (5.94)

3-2-FT-IR spectra

This instrument of analyses is an important tool to identify the chelation mode and the place of coordination. FT−IR spectra of free AMX drug and their complexes **1**–**5** are shown in Fig. 3 and the band assignments are refereed in Table 2.

i. In case of AMX free drug, there are two characteristic bands at 3461 and 3187 cm^{-1}, that can be assigned to $\nu_{(O–H)}$ and $\nu_{(N–H)}$, respectively [47]. These bands are absent or shifted to lower wave numbers in AMX complexes **1**–**4** due to the participated in binding towards metal ions.
ii. In the free AMX drug the stretching vibration bands of phenolic –OH and –CH benzene ring are overlapped in complexation within the range of 3000–3500 cm^{-1}. These results denied the bonding through the –OH phenolic group.
iii. The stretching vibration band $\nu_{(C=C)}$ of benzene ring is presented at 1516 cm^{-1} in case of free AMX drug, this band is exhibiting at the same frequency ~ 1513 cm^{-1} in case of AMX complexes **1**–**4**.

iv. The carbonyl group of β-lactam ring presence at 1776 cm^{-1} in case of free AMX drug, this band $\nu_{(C=O)}$ (β-lactam) is absent or shifted to lower wave numbers in case of the IR spectra of the AMX complexes **1**–**4** due to the involvement in the coordination toward the metal ion [48].

v. The amido group is existed at 1687 cm^{-1} in the free AMX drug, this band was shifted to lower wave numbers at 1641, 1611, 1648 and 1635 cm^{-1} for the AMX complexes **1**–**4**. These data prove that the –NH-CO amido group sharing in the coordination fashion.

vi. The –COOH carboxylic group band in case of AMX free drug is presently at 1713 cm^{-1}, this band was absent in the spectra of the AMX complexes **1**–**4**. This data can be assigned to the deprotonation of carboxylic group by sodium metal in the neutralization state. The difference wave numbers between $\Delta\nu = \nu_{as}COO^- - \nu_sCOO^-$) asymmetric and symmetric stretching vibrations of carboxylic group is larger than >200 cm^{-1}, this data supported the formation of ionic bonds [49] between carboxylic and sodium metal ions.

vii. The presence of bands at 500–600 cm^{-1} are assigned to the $\nu_{(M–O)}$ stretching, vibration bands between metal ions and oxygen's of the carbonyl group.

viii. The bands within the range of 500–400 cm^{-1} are assigned to $\nu_{(M-N)}$ stretching, vibration bands between metal ions and amino group. The infrared spectroscopic results supported that AMX drug acts as a 1:2 tridentate ligand molecule with respect metal ions via amino, amido and β-lactamic groups.

ix. In AMX complexes, the distinguish band at ~ 3400 cm^{-1} with a broad intensity is assigned to the presence of the water molecules inside or outside coordination sphere.

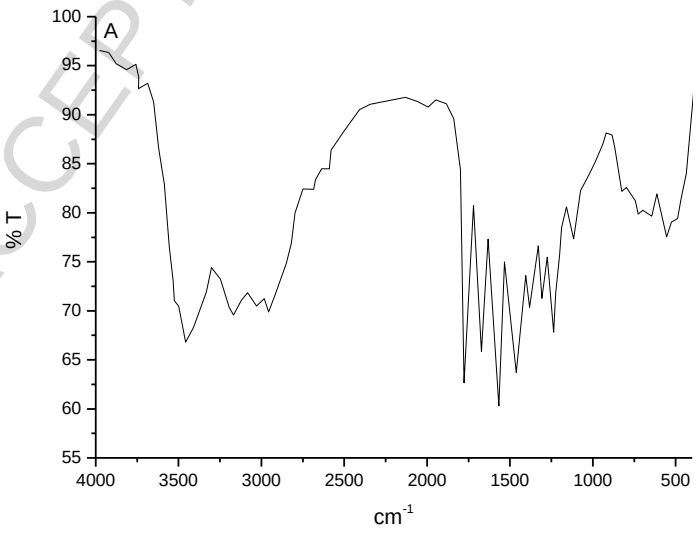

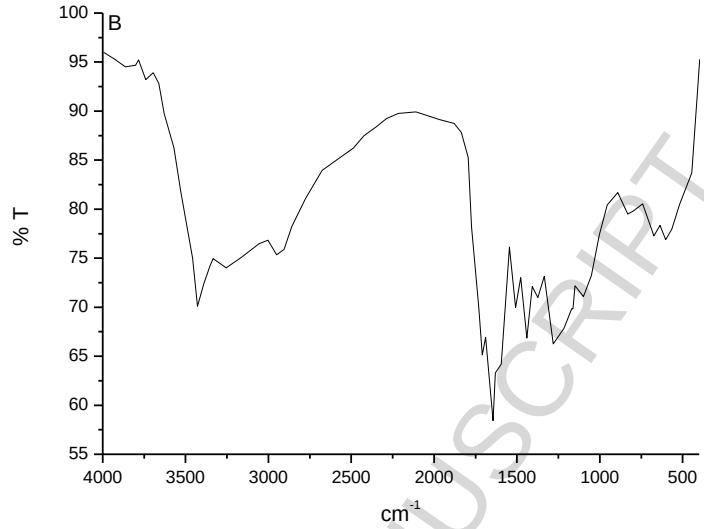

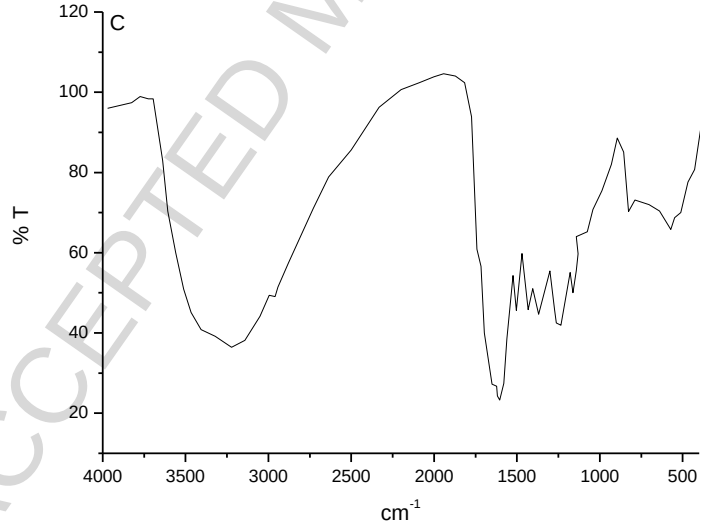

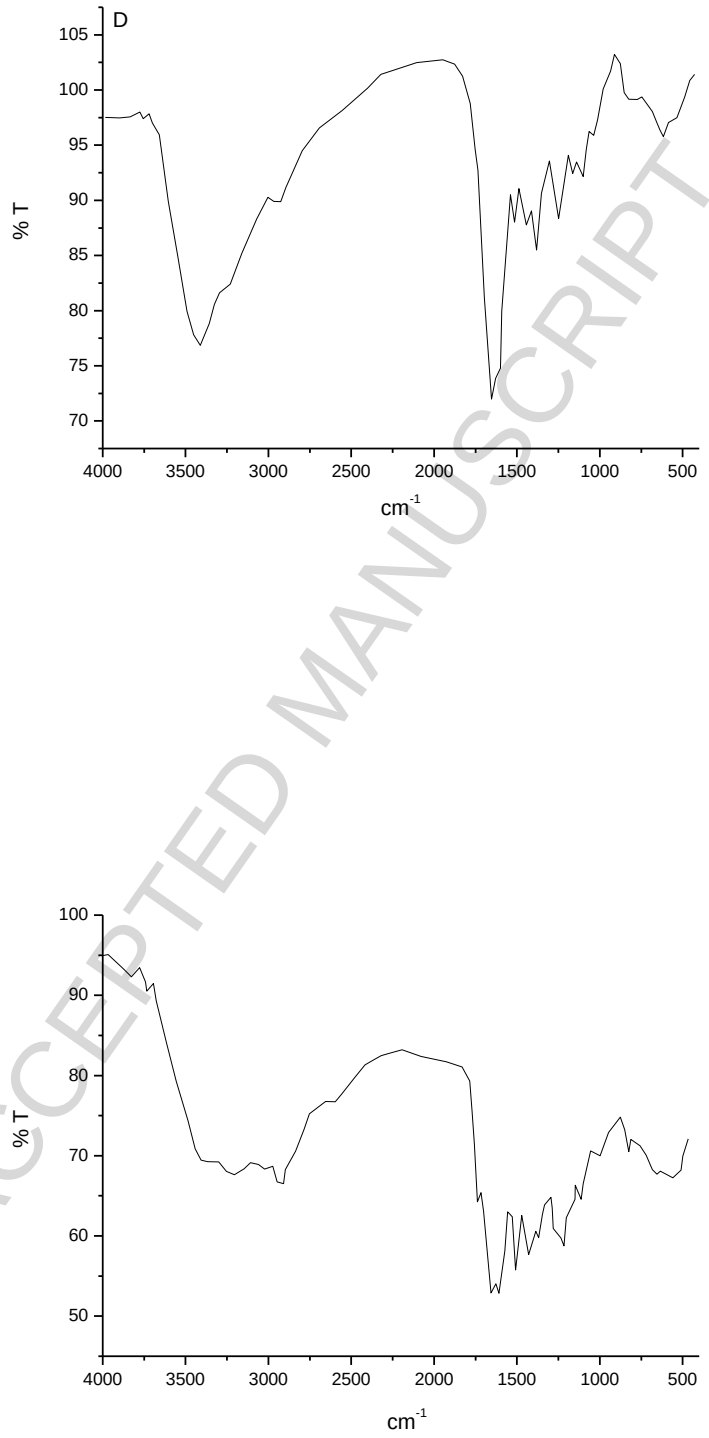

Fig. 3A–E: FT–IR spectra of AMX free drug and complexes **1**–**4**

Table 2: Main FT–IR spectral bands and their assignments of a free AMX drug and their complexes **1**–**4**.

AMX	Cu(II)	Co(II)	Ni(II)	Fe(III)	Assignments
3461	3421	3403	3415	3403	ν(OH); COOH+H_2O

3187	-	-	-	-	ν(NH)
1776	1709 sh	-	-	1739 sh	ν(C=O); β-lactam
1687	1641	1611	1648	1635	ν(C=O); amido group
-	573	575	618	654	ν(M-O)
-	499	500	545	569	ν(M-N)

3-3-Electronic spectra, effective magnetic moments and ESR spectra

The UV–vis absorption spectra of AMX and their complexes **1**–**4** within the range of 200-1000 nm were scanned and assigned. The electronic spectrum of AMX free drug has two characteristic absorption regions at 260-285 nm and 330-370 nm due to the intraligand excitation indicating the effect of the functional groups [50]. Base on chelation, there are some electronic changes due to the interaction of AMX drug with metal ions. The UV-vis. Absorption spectra of AMX complexes **1**–**4** have π→π* transitions at 280–300 nm due to aromaticity of double bond characters [51], and n→π* transitions were exhibit at wavelengths 325–400 nm, that can be assigned to β-lactam, carboxylate, amino, amido, and dimethyl thiazolidine groups [52].

*Cu(II) complex **1***

The reflectance spectra of Cu(II) complex **1** has two distinguish bands exhibited at 15873 and 20618 cm^{-1} that can be assigned to $^2E_g \rightarrow {}^2T_{2g}$ and $^2B_{1g} \rightarrow {}^2A_{1g}$ transitions, respectively. The octahedral geometry around Cu(II) ions is additionally proved by estimation of the effective magnetic moment (μ_{eff}). The experimental μ_{eff} of Cu(II) complex **1** has 1.88 BM, that matched with octahedral structure [53]. The magnetic moment values are excluded any metal–metal interaction with neighbor moieties. The electron spin resonance spectrum of Cu(II)–AMX complex **1** scanned as a polycrystalline samples Figs. 4. The experimental data show that $g_{\parallel}$ =1.8601 and $g_{\perp}$ = 1.7619. The values of both $g_{\parallel}$ and $g_{\perp}$ are less than 2. This suggestion due to octahedral geometry of the copper(II) complex **1**. The $G = (g_{\parallel} - 2)/(g_{\perp} - 2)$, which measure the exchange interaction between the copper centers in a polycrystalline solid has been calculated. According to Hathaway [54, 55], if $G > 4$, the exchange interaction is negligible,but $G < 4$ indicates considerable exchange interaction in the solid complexes. In case of copper(II) complex **1**, the '*G*' value less than 4 indicating the exchange interaction in solid complex. For transition metal compounds,large variations arise in the values of g-factor because of loss of orbital degeneracy and spin-orbit coupling. The value of *g*-factor in transition metal complex gives very important information about the structure of the complex. The molecular orbital coefficients α^2 and β^2 for identify to (covalence of in–plane σ–bonding between 3d and ligand orbitals) and (covalence in–plane π–bonding), respectively, were estimated by using the following relationships [56];

$$\alpha^2 = \left(\frac{A_{\parallel}}{0.036}\right) + \left(g_{\parallel} - 2.0023\right) + \frac{3}{7}(g_{\perp} - 2.0023) + 0.04$$

$$\beta^2 = \frac{(g - 2.9923)E}{-8\lambda\alpha^2}$$

Where, λ =−828 cm^{-1} for the free copper(II) ion and E is the electronic transition energy. The lower value of β^2 compared to α^2 indicates that the in–plane π–bonding is more covalent than the in–plane σ–bonding, the data in a good agreement with

literature [54, 55]. The α^2 value for copper(II) complex indicates a considerable covalency in the bonding between the Cu(II) ion and the AMX ligand.

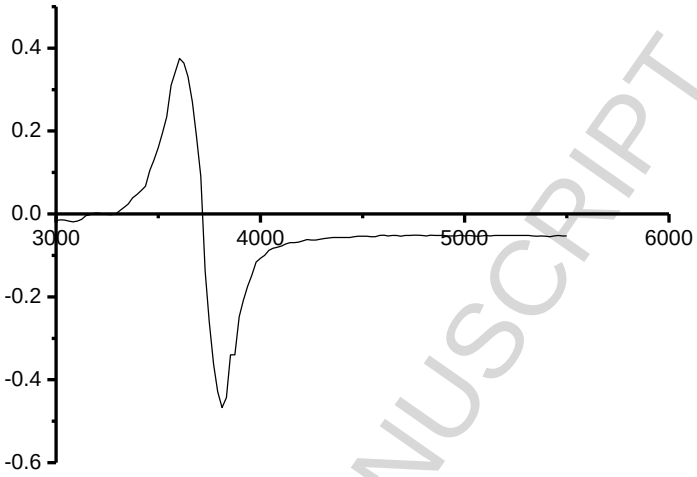

Fig. 4: ESR spectrum of Cu(II)−AMX complex **1**.

*Co(II) complex **2***

The electronic spectrum of cobalt(II) complex **2** has three absorption bands at 12345, 15504 and 18182 cm^{-1}, which can be attributed to $^4T_{1g}(F)\rightarrow{}^4T_{2g}(F)$ (ν1), $^4T_{1g}(F)\rightarrow{}^4A_{2g}(F)$ (ν2) and $^4T_{1g}(F)\rightarrow{}^4T_{1g}(P)$ (ν3), respectively, based on the octahedral geometrical structure [57]. The octahedral geometry of cobalt(II) complex is further supported by the value of the ν2/ν1 ratio, which is 1.26 [58]. The ligand field parameters such as the Racah iner−electronic repulsion parameter (B' = 798 cm^{-1}), ligand field splitting energy ($10D_q$ = 11083), covalency factor (β = 0.810) and ligand field stabilization energy (LFSE = 13.30 kcal. mol^{-1}) have been calculated [58]. For the Co(II) complex, the Racah Racah inner−electronic repulsion parameter (B') is calculated based on the following relationship [58];

$$B' = 1/510\ \{7(\nu3-2\ \nu2) + 3[81\ \nu3^2 - 16\ \nu2(\nu2-\nu3)]^{0.5}\}$$

The ligand field splitting energy ($10D_q$) is estimated from the following relationship;

$$10D_q = 1/3\ (\nu2-\nu3) + 15B'$$

The covalency factor (β) is resulted from the following relationship;

$$\beta = B'/B \text{ (B is the free cobalt ion)}$$

The ligand field stabilization energy (LFSE) is calculated from the following relationship;

$$LFSE = 10D_q$$

The *B′* value is lower than free ion (985 cm^{-1}), that is due to orbital overlap and delocalization of d–orbital. The covalency factor (*β*) is less than unity, this can be assigned upon the metal–ligand bonds have a considerable of covalent character.

The magnetic moment of the Co(II) complex is 4.86 B.M, which is characteristic for an octahedral environment.

*Ni(II) complex **3***

The electronic absorption spectrum of Ni(II) complex **3** exhibit three bands at 25641, 17544 and 11976 cm^{-1} which attributed to $^3A_{2g}(F) \rightarrow {}^3T_{1g}$ (P), (ν3), $^3A_{2g} \rightarrow {}^3T_{1g}$ (F), (ν2) and $^3A_{2g} \rightarrow {}^3T_{2g}$ (F), (ν1), respectively, due to octahedral geometry [59]. Beside of these three bands, there is a charge transfer band is existed at 29412 cm^{-1}. The Racah inter-electronic repulsion parameter (*B′*= 593 cm^{-1}), ligand field splitting energy (10Dq= (ν1) 11976 cm^{-1}), covalency factor (β = 0.5711) and ligand field stabilization energy (LFSE = 14.371 kcal. mol^{-1}) has been calculated. Both 10Dq and B parameters were calculated upon following equations [60-62];

$$B' = (2\,\nu1^2 + \nu2^2 - 3\,\nu1\,\nu2) / (15\,\nu2 - 27\,\nu1)$$

$$\beta = B'/B \text{ (where, B is the free nickel ion = 1038 } cm^{-1})$$

$$LFSE = 12Dq$$

The percentage lowering of energy in free gaseous ion (β^o = 42.89%) is calculated from the following relationship;

$$\beta^o = 100 - (\beta \times 100)$$

The fraction of ν2/ν1 (1.4649 cm^{-1}) is found at the limit of octahedral geometry [60, 61]. The low values of ν2/ν1 are due to the strong interaction between $^3T_{1g}$ (P) and $^3T_{1g}$ (F) states.

The effective magnetic moment μ_{eff} data of Ni(II) complex **3** is 3.45 BM within the high spin octahedral (3.00-3.50 BM). The high spin data are due to arise from the spin orbit coupling which causes an orbital contribution to the quenched $^3A_{2g}$ ground state of Ni(II) ion in an octahedral structure [60].

*Fe(III) complex **4***

The observed magnetic moment of iron(III) complex **4** is 5.82 B.M. Within the accepted range and hence an octahedral geometry, involving d^2sp^3 hybridization [60]. The solid reflectance spectrum of iron(III)–AMX complex **4** has a band at 21276 cm^{-1} that can be assigned to $^6A_{1g} \rightarrow T_{2g}$ (G) transition.

3-4- TG–DTG analyses and calculation of thermodynamic parameters

The TGA–DrTGA thermal analyses curves of AMX complexes **1**–**4** are refereed in Figs. 5A–D and the interpretation of mass loss (%) with various temperature ranges are assigned in Table 3. The thermal decomposition mechanisms of $[M(AMX\text{-}Na)_2].xCl.yH_2O$ (where M= Cu^{2+} (*x*= 2, *y*= 4), Co^{2+} (*x*= 2, *y*= 2), Ni^{2+} (*x*= 2, *y*= 1) and Fe^{3+} (*x*= 3, *y*= 0) complexes can be deduced as follows:

i- $[Cu(AMX–Na)_2)].Cl_2.4H_2O \xrightarrow{50–140^oC}$

$$[Cu(AMX{-}Na)_2)].Cl_2 + 4H_2O$$

$$[Cu(AMX{-}Na)_2)].Cl_2 \xrightarrow{140\text{–}800^{o}C} Cl_2 + AMX{-}Na\ (dec.) + CuO\downarrow + 8C$$

ii- $$[Co(AMX{-}Na)_2)].Cl_2.2H_2O \xrightarrow{50\text{–}120^{o}C} [Co(AMX{-}Na)_2)].Cl_2 + 2H_2O$$

$$[Co(AMX{-}Na)_2)].Cl_2 \xrightarrow{120\text{–}800^{o}C} Cl_2 + AMX{-}Na\ (dec.) + CoO\downarrow + 22C$$

iii- $$[Ni(AMX{-}Na)_2)].Cl_2.\ H_2O \xrightarrow{50\text{–}150^{o}C} [Ni(AMX{-}Na)_2)].Cl_2 + 2H_2O$$

$$[Ni(AMX{-}Na)_2)].Cl_2 \xrightarrow{150\text{–}800^{o}C} Cl_2 + AMX{-}Na\ (dec.) + NiO\downarrow + 23C$$

iv- $$[Fe(AMX{-}Na)_2)].Cl_3 \xrightarrow{150\text{–}800^{o}C} 1½Cl_2 + AMX{-}Na\ (dec.) + FeO\downarrow + 3C$$

Generally, the thermal decomposition of copper(II), cobalt(II), nickel(II) and iron(III) complexes **1**–**4** of AMX is operated under nitrogen atmosphere. These complexes do not have coordinated water molecules, but contain 0–4 uncoordinated water molecules. The crystallized water molecules were liberated in one step (first step 50–150 ^{o}C). The dehydrated complexes exhibited transition phases and decomposition of AMX located in the second and subsequent steps. The final residual products were identified as the respected metal oxides polluted with carbon atoms.

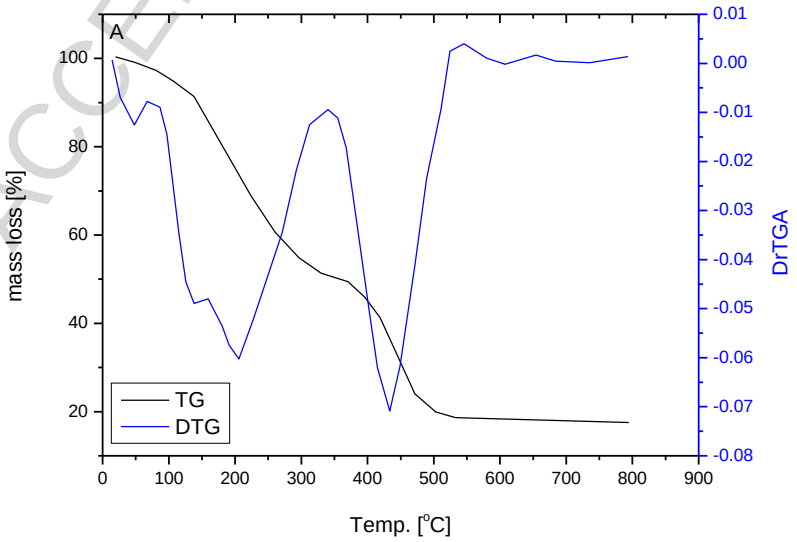

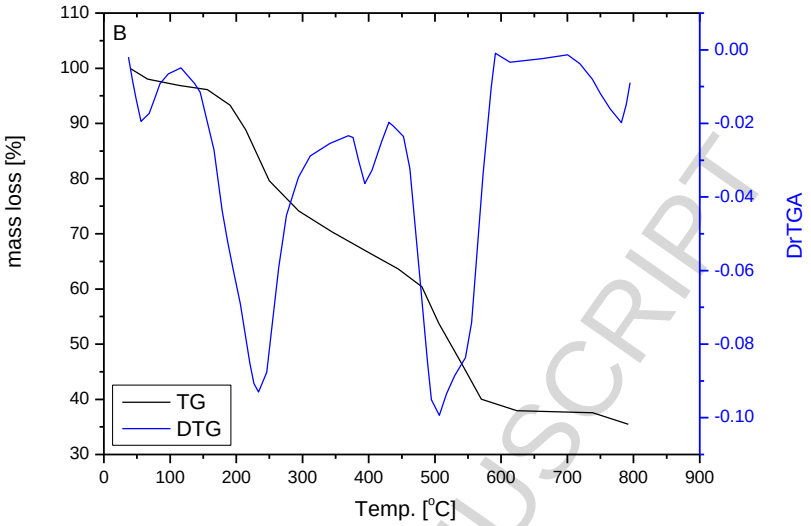

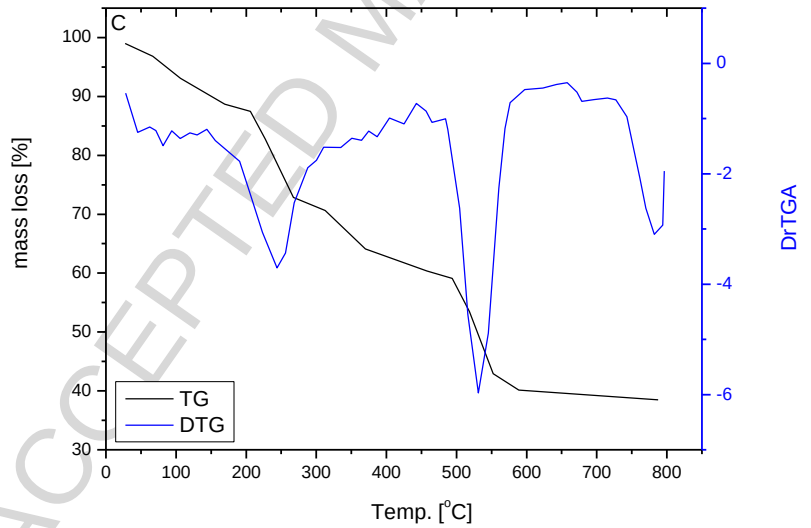

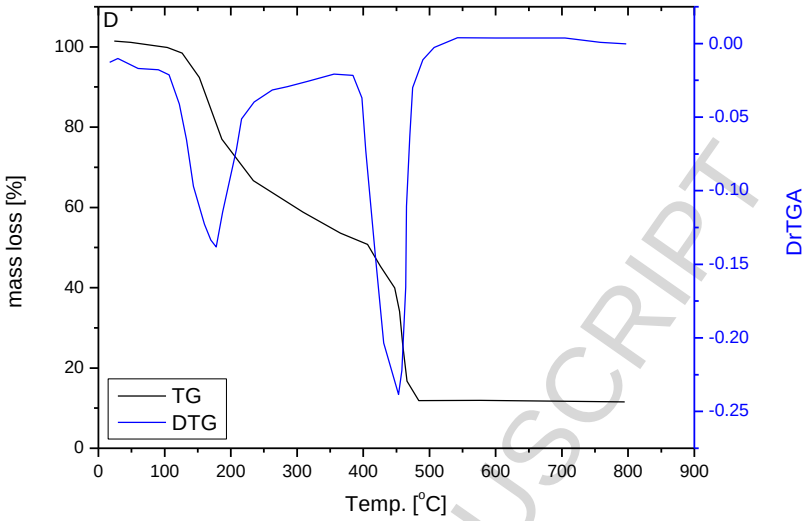

Fig. 5A–E: TGA–DrTGA curves of AMX complexes **1**–**4**

Table 3: Thermo gravimetric assignments of AMX complexes **1**–**4**

Complex	Steps	DTG_{max}/ (°C)	Assignments	Weight loss, % Found (Calcd.)
1	1st	46, 138	$4H_2O$	7.39(7.34)
	2nd	205, 434	Cl_2+AMX-Na (dec.)	75.10(74.77)
	residue		CuO+8C	17.51(17.89)
2	1st	56	$2H_2O$	3.81(3.83)
	2nd	233, 394, 506, 782	Cl_2+AMX-Na (dec.)	60.55(60.14)
	residue		CoO+22C	35.64(36.03)
3	1st	80	H_2O	1.74(1.95)
	2nd	242, 529, 780	Cl_2+AMX-Na (dec.)	59.76(60.03)
	residue		NiO+23C	38.50(38.02)
4	1st	176, 453	1½Cl_2+AMX-Na (dec.)	88.45(88.49)
	residue		FeO+3C	11.55(11.51)

The thermodynamic parameters were calculated theoretically based on the integral Coats & Redfern and Horowitz-Metzger method [63, 64]. The ΔH, ΔS and ΔG parameters were calculated using the relationships; $\Delta H = E - RT$, $\Delta S = R[\ln(Ah/kT)]$ and $\Delta G = \Delta H - T\Delta S$, where, k is the Boltzmann's constant and h is the Planck's constant. The thermodynamic parameters are listed in Table 4.

Table 4: Kinetic parameters using the Coats–Redfern (CR) and Horowitz-Metzger (HM) methods for the AMX complexes **1**–**4**

Complexes	DTG_{max}	Thermodynamic parameters		
		Parameters	Methods	
			CR	HM

Complex **1**	205 °C	E ($Jmol^{-1}$)	$7.99*10^4$	$8.34*10^4$
		A (s^{-1})	$2.61*10^2$	$1.31*10^7$
		ΔS ($Jmol^{-1}K^{-1}$)	$-2.03*10^2$	$-1.13*10^2$
		ΔH ($Jmol^{-1}$)	$3.19*10^4$	$7.94*10^4$
		ΔG ($Jmol^{-1}$)	$9.40*10^4$	$1.33*10^5$
		r	0.989	0.968
Complex **2**	233 °C	E ($Jmol^{-1}$)	$1.41*10^4$	$1.89*10^4$
		A (s^{-1})	$1.89*10^3$	$9.35*10^7$
		ΔS ($Jmol^{-1}K^{-1}$)	$-3.05*10^2$	$-3.86*10^2$
		ΔH ($Jmol^{-1}$)	$6.36*10^3$	$6.48*10^3$
		ΔG ($Jmol^{-1}$)	$2.32*10^4$	$4.34*10^4$
		r	0.991	0.999
Complex **3**	242 °C	E ($Jmol^{-1}$)	$1.99*10^4$	$1.93*10^4$
		A (s^{-1})	$1.03*10^{15}$	$8.92*10^7$
		ΔS ($Jmol^{-1}K^{-1}$)	$-3.42*10^2$	$-3.69*10^2$
		ΔH ($Jmol^{-1}$)	$6.51*10^3$	$6.69*10^3$
		ΔG ($Jmol^{-1}$)	$3.41*10^4$	$2.91*10^4$
		r	0.999	0.999
Complex **4**	176 °C	E ($Jmol^{-1}$)	$1.98*10^4$	$1.34*10^4$
		A (s^{-1})	$2.50*10^1$	$2.31*10^7$
		ΔS ($Jmol^{-1}K^{-1}$)	$-2.26*10^2$	$-1.11*10^2$
		ΔH ($Jmol^{-1}$)	$5.94*10^3$	$1.28*10^4$
		ΔG ($Jmol^{-1}$)	$1.61*10^4$	$2.10*10^4$
		r	0.979	0.979

The activation thermodynamic parameters, such as, energy of activation, enthalpy, entropy and free energy change of the complexes were evaluated and the stabilities of the thermal decomposition of the complexes are discussed. From the kinetic point of view, it is found that the thermal stability of the complexes follows the order Cu(II)>Ni(II)> Fe(III)>Co(II). The reactions for which ΔG is positive and ΔS is negative considered as unfavorable or non spontaneous reactions [65, 66]. The correlation coefficients of the Arrhenius plots of the thermal decomposition steps were found to lie in the range 0.999 to 0.968, showing a good fit with linear functions.

3-5- Theoretical and molecular docking calculation

The molecular structures of the AMX drug and their Cu(II), Co(II), Ni(II) and Fe(III) complexes **1**–**4** are optimized by an HF method with a 3-21G basis set. The molecules were built with the Perkin Elmer ChemBio Draw and optimized using Perkin Elmer ChemBio3D software [67]. The calculated of internal coordinates of molecular structures for AMX and complexes **1**–**4** are shown in Figs. 1 and 2. Selected geometric parameters,bond lengths and bond angles are summarized in Tables 5-8.

The docking process in which the ligand–protein interaction energies are calculated using a Docking Server [68]. The MMFF94 Force field was used for energy minimization of the ligand molecule using Docking Server. Gasteiger partial charges were added to the ligand atoms. Non-polar hydrogen atoms were merged, and rotatable bonds were defined. Docking calculations were carried out on 2q7k-hormone protein model. Essential hydrogen atoms, Kollman united atom type

charges, and solvation parameters were added with the aid of AutoDock tools [69]. Affinity (grid) maps of 20×20×20 Å grid points and 0.375 Å spacing were generated using the Autogrid program [67]. Auto Dock parameter set- and distance-dependent dielectric functions were used in the calculation of the van der Waals and the electrostatic terms, respectively. The molecular docking is a key tool in computational drug design [68]. The focus of molecular docking is to simulate the molecular recognition process. Molecular docking aims to achieve an optimized conformation for both the protein and drug with a relative orientation between them such that the free energy of the overall system is minimized [68]. The results of molecular docking between AMX drug and receptor of prostate cancer mutant 2q7k-hormone showed a possible arrangement between AMX drug and receptor 2q7k. On a docking study showing a favorable interaction between AMX drug and the receptor 2q7k and the calculated of energy are listed in Table 9 and Fig. 6. The 2D plot curves of docking with ligands are shown in Fig. 7. This interaction could activate apoptosis in cancer cells, energy of interactions with drugs. Binding energies are most widely used mode of measuring binding affinity of drugs. Thus, a decrease in binding energy due to mutation will increase the binding affinity of the AMX drug towards the receptor. The characteristic feature of AMX represents in presence of several active sites available for hydrogen bonding. According to our results, (Fig. 8), HB plot curve indicates that, the AMX drug compound binds to the 2q7k protein with hydrogen bond interactions and decomposed interactions energies in Kcal/mole exist of AMX drug with 2q7k.

Table 5: Internal coordinates parameters of AMX drug

Atom	Bond Atom	Bond Length (A)	Angle Atom	Angle (o)	2nd Angle Atom	2nd Angle (o)	2nd Angle Type
C(15)							
N(19)	C(15)	1.450					
C(18)	N(19)	1.369	C(15)	90.000			
C(16)	N(19)	1.450	C(15)	107.700	C(18)	118.400	Pro-R
C(13)	C(15)	1.523	N(19)	90.000	C(16)	130.638	Dihedral
C(17)	C(16)	1.448	N(19)	112.161	C(15)	50.973	Dihedral
N(11)	C(13)	1.450	C(15)	115.566	C(18)	115.566	Pro-S
S(14)	C(15)	1.815	C(13)	109.000	N(19)	104.000	Pro-R
O(20)	C(18)	1.208	C(13)	132.532	N(19)	132.532	Pro-S
C(23)	C(16)	1.509	C(17)	108.773	N(19)	108.773	Pro-R
H(37)	C(16)	1.113	C(17)	107.906	N(19)	107.906	Pro-S
C(9)	N(11)	1.369	C(13)	120.000	C(15)	-94.678	Dihedral
C(21)	C(17)	1.523	S(14)	112.806	C(16)	112.806	Pro-S
C(22)	C(17)	1.523	S(14)	117.399	C(16)	117.399	Pro-R
O(25)	C(23)	1.338	C(16)	120.000	C(17)	-0.000	Dihedral
H(35)	C(13)	1.113	N(11)	96.389	C(15)	124.021	Pro-R
H(36)	C(15)	1.113	C(13)	119.594	S(14)	108.464	Pro-R
C(8)	C(9)	1.509	N(11)	120.000	C(13)	180.000	Dihedral
C(4)	C(8)	1.497	C(9)	109.442	N(11)	119.964	Dihedral
C(3)	C(4)	1.395	C(8)	119.998	C(9)	120.000	Dihedral
C(5)	C(4)	1.395	C(3)	120.003	C(8)	119.998	Pro-S
C(2)	C(3)	1.395	C(4)	120.000	C(5)	0.001	Dihedral
C(1)	C(2)	1.395	C(3)	119.997	C(4)	-0.006	Dihedral
C(6)	C(5)	1.395	C(4)	119.997	C(3)	0.003	Dihedral
O(7)	C(1)	1.355	C(2)	119.999	C(6)	119.999	Pro-R

N(10)	C(8)	1.438	C(4)	109.442	C(9)	109.500	Pro-S
O(12)	C(9)	1.208	C(8)	120.000	N(11)	120.000	Pro-S
O(24)	C(23)	1.208	C(16)	120.000	O(25)	120.000	Pro-R
H(26)	C(2)	1.100	C(1)	120.002	C(3)	120.002	Pro-S
H(27)	C(3)	1.100	C(2)	120.000	C(4)	120.000	Pro-R
H(28)	C(5)	1.100	C(4)	120.001	C(6)	120.001	Pro-S
H(29)	C(6)	1.100	C(1)	120.000	C(5)	120.000	Pro-S
H(31)	C(8)	1.113	C(4)	109.520	C(9)	109.462	Pro-R
H(30)	O(7)	0.972	C(1)	108.000	C(2)	180.000	Dihedral
H(32)	N(10)	1.020	C(8)	109.470	C(4)	180.000	Dihedral
H(33)	N(10)	1.034	C(8)	110.022	H(32)	104.757	Pro-S
H(34)	N(11)	1.012	C(9)	120.000	C(13)	120.000	Pro-S
H(38)	C(21)	1.113	C(17)	109.500	S(14)	73.115	Dihedral
H(39)	C(21)	1.114	C(17)	110.414	H(38)	107.607	Pro-S
H(40)	C(21)	1.114	C(17)	112.171	H(38)	107.438	Pro-R
H(41)	C(22)	1.113	C(17)	109.500	S(14)	113.028	Dihedral
H(42)	C(22)	1.111	C(17)	112.271	H(41)	107.992	Pro-S
H(43)	C(22)	1.114	C(17)	111.379	H(41)	107.051	Pro-R
H(44)	O(25)	0.972	C(23)	106.100	C(16)	180.000	Dihedral

Table 6: Internal coordinates parameters of complex **1**

Atom	Bond Atom	Bond Length (A)	Angle Atom	Angle (^{O})	2nd Angle Atom	2nd Angle (^{O})	2nd Angle Type
C(15)							
N(19)	C(15)	1.448					
C(18)	N(19)	1.355	C(15)	100.468			
C(16)	N(19)	1.447	C(15)	119.429	C(18)	129.648	Pro-R
C(23)	C(16)	1.505	N(19)	121.032	C(15)	175.674	Dihedral
C(17)	C(16)	1.547	N(19)	102.921	C(23)	115.023	Pro-R
O(24)	C(23)	1.206	C(16)	140.518	C(17)	-77.270	Dihedral
Cu(26)	O(24)	1.810	C(23)	107.421	C(16)	164.380	Dihedral
O(25)	Cu(26)	1.849	O(24)	64.022	C(23)	2.073	Dihedral
O(50)	Cu(26)	1.811	O(25)	88.790	C(23)	129.888	Dihedral
O(51)	Cu(26)	1.849	O(25)	122.061	C(23)	71.676	Dihedral
C(49)	O(50)	1.205	Cu(26)	107.459	O(25)	-125.857	Dihedral
C(42)	C(49)	1.503	O(50)	143.099	O(51)	123.062	Pro-R
N(45)	C(42)	1.439	C(49)	116.656	O(50)	-135.301	Dihedral
C(41)	N(45)	1.447	C(42)	121.761	C(49)	173.105	Dihedral
C(44)	N(45)	1.352	C(41)	102.064	C(42)	132.240	Pro-S
C(43)	C(42)	1.551	N(45)	102.937	C(49)	118.016	Pro-R
C(13)	C(15)	1.599	N(19)	83.496	C(16)	-148.556	Dihedral
S(14)	C(15)	1.823	C(13)	116.903	N(19)	100.917	Pro-R
C(39)	C(41)	1.599	N(45)	82.323	C(42)	-161.616	Dihedral
S(40)	C(41)	1.817	C(39)	119.755	N(45)	97.529	Pro-R
N(11)	C(13)	1.460	C(15)	114.702	C(18)	110.136	Pro-S
C(21)	C(17)	1.537	S(14)	109.936	C(16)	111.566	Pro-S
C(22)	C(17)	1.541	S(14)	108.270	C(16)	111.864	Pro-R
N(37)	C(39)	1.467	C(41)	117.360	C(44)	118.121	Pro-S
C(47)	C(43)	1.540	S(40)	108.740	C(42)	110.864	Pro-S
C(48)	C(43)	1.540	S(40)	108.771	C(42)	113.180	Pro-R
O(20)	C(18)	1.199	C(13)	138.087	N(19)	132.642	Pro-S
O(46)	C(44)	1.199	C(39)	140.619	N(45)	131.640	Pro-S
C(9)	N(11)	1.364	C(13)	122.075	C(15)	73.283	Dihedral
C(35)	N(37)	1.368	C(39)	124.632	C(41)	-75.687	Dihedral

C(8)	C(9)	1.517	N(11)	114.047	C(13)	-168.892	Dihedral
C(4)	C(8)	1.514	C(9)	113.165	N(11)	-39.482	Dihedral
C(3)	C(4)	1.345	C(8)	120.071	C(9)	85.370	Dihedral
C(5)	C(4)	1.344	C(3)	117.564	C(8)	122.364	Pro-R
C(2)	C(3)	1.340	C(4)	121.436	C(5)	-0.499	Dihedral
C(1)	C(2)	1.343	C(3)	121.044	C(4)	-0.208	Dihedral
C(6)	C(5)	1.342	C(4)	120.866	C(3)	1.048	Dihedral
O(7)	C(1)	1.360	C(2)	121.483	C(6)	120.982	Pro-R
N(10)	C(8)	1.470	C(4)	111.354	C(9)	109.995	Pro-S
O(12)	C(9)	1.205	C(8)	123.443	N(11)	122.471	Pro-R
C(34)	C(35)	1.520	N(37)	113.476	C(39)	174.161	Dihedral
C(30)	C(34)	1.512	C(35)	112.852	N(37)	176.497	Dihedral
C(29)	C(30)	1.345	C(34)	120.869	C(35)	101.828	Dihedral
C(31)	C(30)	1.344	C(29)	117.875	C(34)	121.215	Pro-S
C(28)	C(29)	1.342	C(30)	121.071	C(31)	0.259	Dihedral
C(27)	C(28)	1.343	C(29)	121.262	C(30)	-0.615	Dihedral
C(32)	C(31)	1.341	C(30)	120.736	C(29)	0.068	Dihedral
O(33)	C(27)	1.361	C(28)	121.629	C(32)	120.851	Pro-S
N(36)	C(34)	1.469	C(30)	110.130	C(35)	109.786	Pro-S
O(38)	C(35)	1.204	C(34)	123.222	N(37)	123.299	Pro-S
H(52)	C(2)	1.103	C(1)	119.411	C(3)	119.538	Pro-S
H(53)	C(3)	1.102	C(2)	118.626	C(4)	119.935	Pro-S
H(54)	C(5)	1.101	C(4)	120.821	C(6)	118.310	Pro-S
H(55)	C(6)	1.103	C(1)	119.079	C(5)	119.370	Pro-R
H(70)	C(28)	1.103	C(27)	119.206	C(29)	119.519	Pro-R
H(71)	C(29)	1.103	C(28)	118.863	C(30)	120.043	Pro-R
H(72)	C(31)	1.102	C(30)	120.522	C(32)	118.722	Pro-R
H(73)	C(32)	1.102	C(27)	119.168	C(31)	119.189	Pro-S
H(62)	C(15)	1.109	C(13)	116.314	S(14)	119.259	Pro-R
H(80)	C(41)	1.109	C(39)	116.787	S(40)	118.952	Pro-R
H(61)	C(13)	1.110	N(11)	114.826	C(15)	115.469	Pro-R
H(63)	C(16)	1.119	C(17)	108.421	N(19)	105.515	Pro-S
H(79)	C(39)	1.113	N(37)	110.704	C(41)	111.825	Pro-R
H(81)	C(42)	1.117	C(43)	109.051	N(45)	105.628	Pro-S
H(57)	C(8)	1.117	C(4)	109.692	C(9)	105.655	Pro-R
H(60)	N(11)	1.020	C(9)	118.885	C(13)	118.763	Pro-S
H(75)	C(34)	1.117	C(30)	110.093	C(35)	106.557	Pro-R
H(78)	N(37)	1.020	C(35)	116.585	C(39)	118.661	Pro-R
H(56)	O(7)	0.971	C(1)	108.931	C(2)	174.395	Dihedral
H(58)	N(10)	1.035	C(8)	110.108	C(4)	-179.954	Dihedral
H(59)	N(10)	1.034	C(8)	110.526	H(58)	104.250	Pro-S
H(64)	C(21)	1.114	C(17)	111.549	S(14)	64.818	Dihedral
H(65)	C(21)	1.113	C(17)	110.811	H(64)	107.629	Pro-S
H(66)	C(21)	1.113	C(17)	111.919	H(64)	107.675	Pro-R
H(67)	C(22)	1.111	C(17)	111.579	S(14)	178.773	Dihedral
H(68)	C(22)	1.114	C(17)	111.736	H(67)	106.969	Pro-S
H(69)	C(22)	1.112	C(17)	112.338	H(67)	106.318	Pro-R
H(74)	O(33)	0.974	C(27)	108.067	C(28)	-142.906	Dihedral
H(76)	N(36)	1.034	C(34)	110.497	C(30)	-60.142	Dihedral
H(77)	N(36)	1.034	C(34)	109.830	H(76)	104.758	Pro-S
H(82)	C(47)	1.114	C(43)	111.559	S(40)	63.503	Dihedral
H(83)	C(47)	1.114	C(43)	110.607	H(82)	107.499	Pro-S
H(84)	C(47)	1.114	C(43)	112.082	H(82)	107.493	Pro-R
H(85)	C(48)	1.111	C(43)	112.184	S(40)	70.791	Dihedral
H(86)	C(48)	1.112	C(43)	111.443	H(85)	107.028	Pro-S
H(87)	C(48)	1.114	C(43)	111.794	H(85)	107.894	Pro-R

Table 7: Internal coordinates parameters of complex **2**

Atom	Bond Atom	Bond Length(A)	Angle Atom	Angle (^{O})	2nd Angle Atom	2nd Angle (^{O})	2nd Angle Type
C(15)							
N(19)	C(15)	1.450					
C(18)	N(19)	1.369	C(15)	90.000			
C(16)	N(19)	1.450	C(15)	107.700	C(18)	118.400	Pro-R
C(13)	C(15)	1.523	N(19)	90.000	C(16)	-130.638	Dihedral
C(23)	C(16)	1.509	N(19)	108.773	C(15)	171.335	Dihedral
N(11)	C(13)	1.450	C(15)	115.566	C(18)	115.566	Pro-S
S(14)	C(15)	1.815	C(13)	109.000	N(19)	104.000	Pro-R
C(17)	C(16)	1.448	N(19)	112.161	C(23)	108.773	Pro-R
O(20)	C(18)	1.208	C(13)	132.532	N(19)	132.532	Pro-S
C(9)	N(11)	1.369	C(13)	120.000	C(15)	-94.678	Dihedral
C(21)	C(17)	1.523	S(14)	112.806	C(16)	112.806	Pro-S
C(22)	C(17)	1.523	S(14)	117.399	C(16)	117.399	Pro-R
O(24)	C(23)	1.208	C(16)	157.690	C(17)	-118.783	Dihedral
H(61)	C(13)	1.113	N(11)	96.389	C(15)	124.021	Pro-R
H(62)	C(15)	1.113	C(13)	119.594	S(14)	108.464	Pro-R
H(63)	C(16)	1.113	C(17)	107.906	N(19)	107.906	Pro-S
Co(51)	O(24)	0.600	C(23)	90.000	C(16)	180.000	Dihedral
O(25)	Co(51)	0.600	O(24)	90.000	C(23)	0.000	Dihedral
O(49)	Co(51)	0.925	O(25)	115.957	C(23)	135.374	Dihedral
O(50)	Co(51)	1.037	O(25)	108.504	C(23)	-117.441	Dihedral
C(48)	O(49)	1.208	Co(51)	90.000	O(25)	90.000	Dihedral
C(41)	C(48)	1.509	O(49)	157.595	O(50)	157.595	Pro-R
N(44)	C(41)	1.450	C(48)	108.773	O(49)	118.783	Dihedral
C(40)	N(44)	1.450	C(41)	107.700	C(48)	171.335	Dihedral
C(43)	N(44)	1.369	C(40)	90.000	C(41)	118.400	Pro-S
C(42)	C(41)	1.448	N(44)	112.161	C(48)	108.773	Pro-R
C(38)	C(40)	1.523	N(44)	90.000	C(41)	-130.638	Dihedral
S(39)	C(40)	1.815	C(38)	109.000	N(44)	104.000	Pro-R
N(36)	C(38)	1.450	C(40)	115.566	C(43)	115.566	Pro-S
C(46)	C(42)	1.523	S(39)	112.806	C(41)	112.806	Pro-S
C(47)	C(42)	1.523	S(39)	117.399	C(41)	117.399	Pro-R
O(45)	C(43)	1.208	C(38)	132.532	N(44)	132.532	Pro-S
C(34)	N(36)	1.369	C(38)	120.000	C(40)	-94.678	Dihedral
C(8)	C(9)	1.509	N(11)	120.000	C(13)	180.000	Dihedral
C(4)	C(8)	1.497	C(9)	109.442	N(11)	119.964	Dihedral
C(3)	C(4)	1.395	C(8)	119.998	C(9)	120.000	Dihedral
C(5)	C(4)	1.395	C(3)	120.003	C(8)	119.998	Pro-R
C(2)	C(3)	1.395	C(4)	120.000	C(5)	0.001	Dihedral
C(1)	C(2)	1.395	C(3)	119.997	C(4)	-0.006	Dihedral
C(6)	C(5)	1.395	C(4)	119.997	C(3)	0.003	Dihedral
O(7)	C(1)	1.355	C(2)	119.999	C(6)	119.999	Pro-S
N(10)	C(8)	1.438	C(4)	109.442	C(9)	109.500	Pro-S
O(12)	C(9)	1.208	C(8)	120.000	N(11)	120.000	Pro-S
C(33)	C(34)	1.509	N(36)	120.000	C(38)	-180.000	Dihedral
C(29)	C(33)	1.497	C(34)	109.442	N(36)	119.964	Dihedral
C(28)	C(29)	1.395	C(33)	119.998	C(34)	120.000	Dihedral
C(30)	C(29)	1.395	C(28)	120.003	C(33)	119.998	Pro-S
C(27)	C(28)	1.395	C(29)	120.000	C(30)	0.001	Dihedral
C(26)	C(27)	1.395	C(28)	119.997	C(29)	-0.006	Dihedral
C(31)	C(30)	1.395	C(29)	119.997	C(28)	0.003	Dihedral

O(32)	C(26)	1.355	C(27)	119.999	C(31)	119.999	Pro-S
N(35)	C(33)	1.438	C(29)	109.442	C(34)	109.500	Pro-S
O(37)	C(34)	1.208	C(33)	120.000	N(36)	120.000	Pro-R
H(52)	C(2)	1.100	C(1)	120.002	C(3)	120.002	Pro-S
H(53)	C(3)	1.100	C(2)	120.000	C(4)	120.000	Pro-R
H(54)	C(5)	1.100	C(4)	120.001	C(6)	120.001	Pro-R
H(55)	C(6)	1.100	C(1)	120.000	C(5)	120.000	Pro-R
H(70)	C(27)	1.100	C(26)	120.002	C(28)	120.002	Pro-R
H(71)	C(28)	1.100	C(27)	120.000	C(29)	120.000	Pro-R
H(72)	C(30)	1.100	C(29)	120.001	C(31)	120.001	Pro-S
H(73)	C(31)	1.100	C(26)	120.000	C(30)	120.000	Pro-R
H(80)	C(40)	1.113	C(38)	119.594	S(39)	108.464	Pro-R
H(79)	C(38)	1.113	N(36)	96.389	C(40)	124.021	Pro-R
H(81)	C(41)	1.113	C(42)	107.906	N(44)	107.906	Pro-S
H(57)	C(8)	1.113	C(4)	109.520	C(9)	109.462	Pro-R
H(75)	C(33)	1.113	C(29)	109.520	C(34)	109.462	Pro-R
H(78)	N(36)	1.012	C(34)	120.000	C(38)	120.000	Pro-R
H(56)	O(7)	0.972	C(1)	108.000	C(2)	180.000	Dihedral
H(58)	N(10)	1.020	C(8)	109.470	C(4)	-180.000	Dihedral
H(59)	N(10)	1.035	C(8)	110.086	H(58)	104.799	Pro-S
H(60)	N(11)	1.012	C(9)	120.000	C(13)	120.000	Pro-S
H(64)	C(21)	1.113	C(17)	109.500	S(14)	73.115	Dihedral
H(65)	C(21)	1.113	C(17)	110.991	H(64)	107.231	Pro-S
H(66)	C(21)	1.113	C(17)	112.155	H(64)	107.442	Pro-R
H(67)	C(22)	1.113	C(17)	109.500	S(14)	113.028	Dihedral
H(68)	C(22)	1.111	C(17)	113.432	H(67)	107.924	Pro-S
H(69)	C(22)	1.113	C(17)	111.325	H(67)	107.669	Pro-R
H(74)	O(32)	0.972	C(26)	108.000	C(27)	-180.000	Dihedral
H(76)	N(35)	1.020	C(33)	109.470	C(29)	-180.000	Dihedral
H(77)	N(35)	1.034	C(33)	109.666	H(76)	104.850	Pro-S
H(82)	C(46)	1.113	C(42)	109.500	S(39)	73.115	Dihedral
H(83)	C(46)	1.114	C(42)	110.582	H(82)	107.183	Pro-S
H(84)	C(46)	1.113	C(42)	112.426	H(82)	107.462	Pro-R
H(85)	C(47)	1.113	C(42)	109.500	S(39)	113.028	Dihedral
H(86)	C(47)	1.114	C(42)	110.903	H(85)	108.222	Pro-S
H(87)	C(47)	1.114	C(42)	111.384	H(85)	106.508	Pro-R

Table 8: Internal coordinates parameters of complex **4**

Atom	Bond Atom	Bond Length (A)	Angle Atom	Angle (^{o})	2nd Angle Atom	2nd Angle (^{o})	2nd Angle Type
C(15)							
N(19)	C(15)	1.450					
C(18)	N(19)	1.369	C(15)	90.000			
C(16)	N(19)	1.450	C(15)	107.700	C(18)	118.400	Pro-R
C(13)	C(15)	1.523	N(19)	90.000	C(16)	-130.638	Dihedral
C(23)	C(16)	1.509	N(19)	108.773	C(15)	171.335	Dihedral
N(11)	C(13)	1.450	C(15)	115.566	C(18)	115.566	Pro-S
S(14)	C(15)	1.815	C(13)	109.000	N(19)	104.000	Pro-R
C(17)	C(16)	1.448	N(19)	112.161	C(23)	108.773	Pro-R
O(20)	C(18)	1.208	C(13)	132.532	N(19)	132.532	Pro-S
C(9)	N(11)	1.369	C(13)	120.000	C(15)	-94.678	Dihedral
C(21)	C(17)	1.523	S(14)	112.806	C(16)	112.806	Pro-S
C(22)	C(17)	1.523	S(14)	117.399	C(16)	117.399	Pro-R
O(24)	C(23)	1.208	C(16)	125.802	C(17)	-118.783	Dihedral
H(86)	C(13)	1.113	N(11)	96.389	C(15)	124.021	Pro-R

H(87)	C(15)	1.113	C(13)	119.594	S(14)	108.464	Pro-R
H(88)	C(16)	1.113	C(17)	107.906	N(19)	107.906	Pro-S
Fe(76)	O(24)	1.810	C(23)	90.000	C(16)	180.000	Dihedral
O(25)	Fe(76)	1.810	O(24)	90.000	C(23)	0.000	Dihedral
O(49)	Fe(76)	1.809	O(25)	127.710	C(23)	-119.785	Dihedral
O(50)	Fe(76)	1.846	O(25)	99.315	C(23)	177.129	Dihedral
O(74)	Fe(76)	1.810	O(25)	90.000	O(50)	180.000	Pro-R
O(75)	Fe(76)	1.810	O(25)	90.000	O(50)	0.000	Pro-R
C(48)	O(49)	1.208	Fe(76)	90.000	O(25)	90.000	Dihedral
C(41)	C(48)	1.509	O(49)	144.227	O(50)	144.227	Pro-S
N(44)	C(41)	1.450	C(48)	108.773	O(49)	118.783	Dihedral
C(40)	N(44)	1.450	C(41)	107.700	C(48)	171.335	Dihedral
C(43)	N(44)	1.369	C(40)	90.000	C(41)	118.400	Pro-S
C(42)	C(41)	1.448	N(44)	112.161	C(48)	108.773	Pro-R
C(73)	O(74)	1.208	Fe(76)	90.000	O(25)	-90.000	Dihedral
C(66)	C(73)	1.509	O(74)	144.227	O(75)	144.227	Pro-S
N(69)	C(66)	1.450	C(73)	108.773	O(74)	-55.603	Dihedral
C(65)	N(69)	1.450	C(66)	107.700	C(73)	171.335	Dihedral
C(68)	N(69)	1.369	C(65)	90.000	C(66)	118.400	Pro-S
C(67)	C(66)	1.448	N(69)	112.161	C(73)	108.773	Pro-R
C(38)	C(40)	1.523	N(44)	90.000	C(41)	-130.638	Dihedral
S(39)	C(40)	1.815	C(38)	109.000	N(44)	104.000	Pro-R
C(63)	C(65)	1.523	N(69)	90.000	C(66)	-130.638	Dihedral
S(64)	C(65)	1.815	C(63)	109.000	N(69)	104.000	Pro-R
N(36)	C(38)	1.450	C(40)	115.566	C(43)	115.566	Pro-S
C(46)	C(42)	1.523	S(39)	112.806	C(41)	112.806	Pro-S
C(47)	C(42)	1.523	S(39)	117.399	C(41)	117.399	Pro-R
N(61)	C(63)	1.450	C(65)	115.566	C(68)	115.566	Pro-S
C(71)	C(67)	1.523	S(64)	112.806	C(66)	112.806	Pro-S
C(72)	C(67)	1.523	S(64)	117.399	C(66)	117.399	Pro-R
O(45)	C(43)	1.208	C(38)	132.532	N(44)	132.532	Pro-R
O(70)	C(68)	1.208	C(63)	132.532	N(69)	132.532	Pro-S
C(34)	N(36)	1.369	C(38)	120.000	C(40)	-94.678	Dihedral
C(59)	N(61)	1.369	C(63)	120.000	C(65)	-94.678	Dihedral
C(8)	C(9)	1.509	N(11)	120.000	C(13)	180.000	Dihedral
C(4)	C(8)	1.497	C(9)	109.442	N(11)	119.964	Dihedral
C(3)	C(4)	1.395	C(8)	119.998	C(9)	120.000	Dihedral
C(5)	C(4)	1.395	C(3)	120.003	C(8)	119.998	Pro-R
C(2)	C(3)	1.395	C(4)	120.000	C(5)	0.001	Dihedral
C(1)	C(2)	1.395	C(3)	119.997	C(4)	-0.006	Dihedral
C(6)	C(5)	1.395	C(4)	119.997	C(3)	0.003	Dihedral
O(7)	C(1)	1.355	C(2)	119.999	C(6)	119.999	Pro-R
N(10)	C(8)	1.438	C(4)	109.442	C(9)	109.500	Pro-S
O(12)	C(9)	1.208	C(8)	120.000	N(11)	120.000	Pro-R
C(33)	C(34)	1.509	N(36)	120.000	C(38)	180.000	Dihedral
C(29)	C(33)	1.497	C(34)	109.442	N(36)	119.964	Dihedral
C(28)	C(29)	1.395	C(33)	119.998	C(34)	120.000	Dihedral
C(30)	C(29)	1.395	C(28)	120.003	C(33)	119.998	Pro-S
C(27)	C(28)	1.395	C(29)	120.000	C(30)	0.001	Dihedral
C(26)	C(27)	1.395	C(28)	119.997	C(29)	-0.006	Dihedral
C(31)	C(30)	1.395	C(29)	119.997	C(28)	0.003	Dihedral
O(32)	C(26)	1.355	C(27)	119.999	C(31)	119.999	Pro-R
N(35)	C(33)	1.438	C(29)	109.442	C(34)	109.500	Pro-S
O(37)	C(34)	1.208	C(33)	120.000	N(36)	120.000	Pro-R
C(58)	C(59)	1.509	N(61)	120.000	C(63)	180.000	Dihedral
C(54)	C(58)	1.497	C(59)	109.442	N(61)	119.964	Dihedral
C(53)	C(54)	1.395	C(58)	119.998	C(59)	120.000	Dihedral
C(55)	C(54)	1.395	C(53)	120.003	C(58)	119.998	Pro-S

C(52)	C(53)	1.395	C(54)	120.000	C(55)	0.001	Dihedral
C(51)	C(52)	1.395	C(53)	119.997	C(54)	-0.006	Dihedral
C(56)	C(55)	1.395	C(54)	119.997	C(53)	0.003	Dihedral
O(57)	C(51)	1.355	C(52)	119.999	C(56)	119.999	Pro-S
N(60)	C(58)	1.438	C(54)	109.442	C(59)	109.500	Pro-S
O(62)	C(59)	1.208	C(58)	120.000	N(61)	120.000	Pro-S
H(77)	C(2)	1.100	C(1)	120.002	C(3)	120.002	Pro-S
H(78)	C(3)	1.100	C(2)	120.000	C(4)	120.000	Pro-R
H(79)	C(5)	1.100	C(4)	120.001	C(6)	120.001	Pro-R
H(80)	C(6)	1.100	C(1)	120.000	C(5)	120.000	Pro-R
H(95)	C(27)	1.100	C(26)	120.002	C(28)	120.002	Pro-R
H(96)	C(28)	1.100	C(27)	120.000	C(29)	120.000	Pro-S
H(97)	C(30)	1.100	C(29)	120.001	C(31)	120.001	Pro-S
H(98)	C(31)	1.100	C(26)	120.000	C(30)	120.000	Pro-R
H(113)	C(52)	1.100	C(51)	120.002	C(53)	120.002	Pro-R
H(114)	C(53)	1.100	C(52)	120.000	C(54)	120.000	Pro-S
H(115)	C(55)	1.100	C(54)	120.001	C(56)	120.001	Pro-R
H(116)	C(56)	1.100	C(51)	120.000	C(55)	120.000	Pro-R
H(105)	C(40)	1.113	C(38)	119.594	S(39)	108.464	Pro-R
H(123)	C(65)	1.113	C(63)	119.594	S(64)	108.464	Pro-R
H(104)	C(38)	1.113	N(36)	96.389	C(40)	124.021	Pro-R
H(106)	C(41)	1.113	C(42)	107.906	N(44)	107.906	Pro-S
H(122)	C(63)	1.113	N(61)	96.389	C(65)	124.021	Pro-R
H(124)	C(66)	1.113	C(67)	107.906	N(69)	107.906	Pro-S
H(82)	C(8)	1.113	C(4)	109.520	C(9)	109.462	Pro-R
H(100)	C(33)	1.113	C(29)	109.520	C(34)	109.462	Pro-R
H(103)	N(36)	1.012	C(34)	120.000	C(38)	120.000	Pro-S
H(118)	C(58)	1.113	C(54)	109.520	C(59)	109.462	Pro-R
H(121)	N(61)	1.012	C(59)	120.000	C(63)	120.000	Pro-S
H(81)	O(7)	0.972	C(1)	108.000	C(2)	180.000	Dihedral
H(83)	N(10)	1.020	C(8)	109.470	C(4)	180.000	Dihedral
H(84)	N(10)	1.034	C(8)	109.865	H(83)	105.325	Pro-S
H(85)	N(11)	1.012	C(9)	120.000	C(13)	120.000	Pro-R
H(89)	C(21)	1.113	C(17)	109.500	S(14)	73.115	Dihedral
H(90)	C(21)	1.113	C(17)	110.784	H(89)	106.868	Pro-S
H(91)	C(21)	1.113	C(17)	112.154	H(89)	106.885	Pro-R
H(92)	C(22)	1.113	C(17)	109.500	S(14)	113.028	Dihedral
H(93)	C(22)	1.110	C(17)	112.751	H(92)	107.715	Pro-S
H(94)	C(22)	1.113	C(17)	110.973	H(92)	107.390	Pro-R
H(99)	O(32)	0.972	C(26)	108.000	C(27)	180.000	Dihedral
H(101)	N(35)	1.020	C(33)	109.470	C(29)	-180.000	Dihedral
H(102)	N(35)	1.035	C(33)	109.839	H(101)	105.528	Pro-S
H(107)	C(46)	1.113	C(42)	109.500	S(39)	73.115	Dihedral
H(108)	C(46)	1.113	C(42)	111.133	H(107)	107.188	Pro-S
H(109)	C(46)	1.114	C(42)	111.919	H(107)	107.526	Pro-R
H(110)	C(47)	1.113	C(42)	109.500	S(39)	113.028	Dihedral
H(111)	C(47)	1.112	C(42)	111.454	H(110)	107.209	Pro-S
H(112)	C(47)	1.114	C(42)	111.370	H(110)	107.307	Pro-R
H(117)	O(57)	0.972	C(51)	108.000	C(52)	-180.000	Dihedral
H(119)	N(60)	1.020	C(58)	109.470	C(54)	180.000	Dihedral
H(120)	N(60)	1.035	C(58)	109.836	H(119)	105.504	Pro-S
H(125)	C(71)	1.113	C(67)	109.500	S(64)	73.115	Dihedral
H(126)	C(71)	1.113	C(67)	110.846	H(125)	106.860	Pro-S
H(127)	C(71)	1.113	C(67)	112.000	H(125)	107.095	Pro-R
H(128)	C(72)	1.113	C(67)	109.500	S(64)	113.028	Dihedral
H(129)	C(72)	1.113	C(67)	111.260	H(128)	107.679	Pro-S
H(130)	C(72)	1.114	C(67)	111.531	H(128)	107.192	Pro-R

Table 9: Energy data produced from molecular docking calculations of AMX drug with receptor prostate cancer mutant 2q7k–hormone

Est. Free energy of binding (kcal/mol)	Est. inhibition constant, K_i (μM)	Electrostatic energy (kcal/mol)	Total intermolecular energy (kcal/mol)	Interact surface
-4.712	443.18	-1.464	4.73	360.777

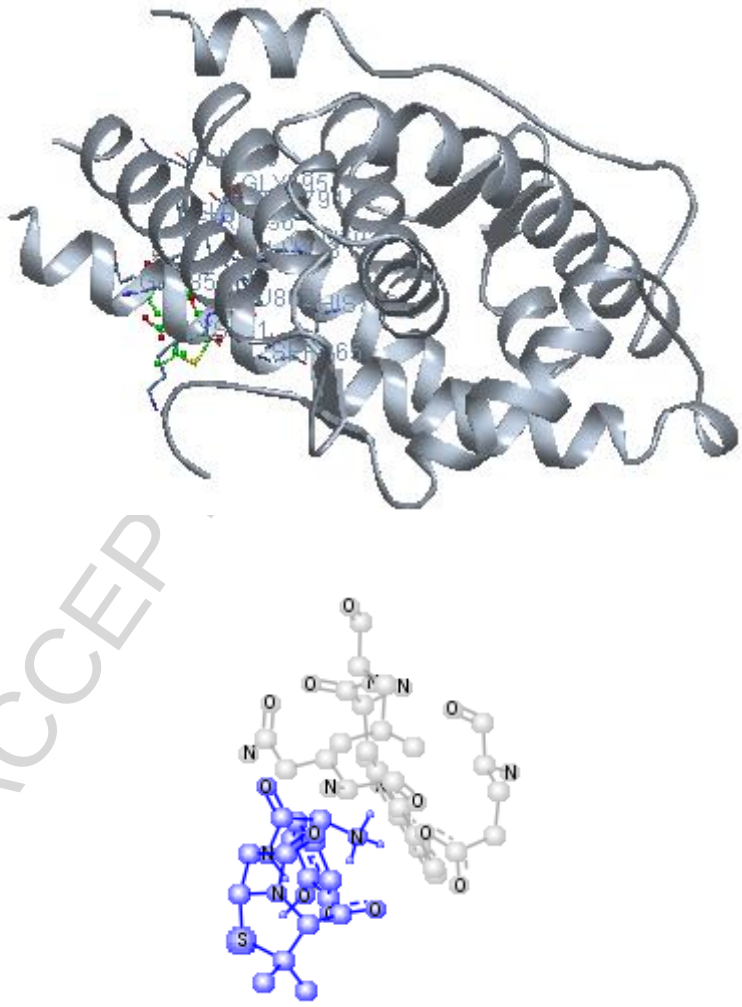

Fig. 6: The AMX drug (green in (A) and blue in (B)) in the interaction with receptor prostate cancer mutant 2q7k–hormone. (For interpretation of the references to color in this figure legend, the reader is referred to the web version of this article).

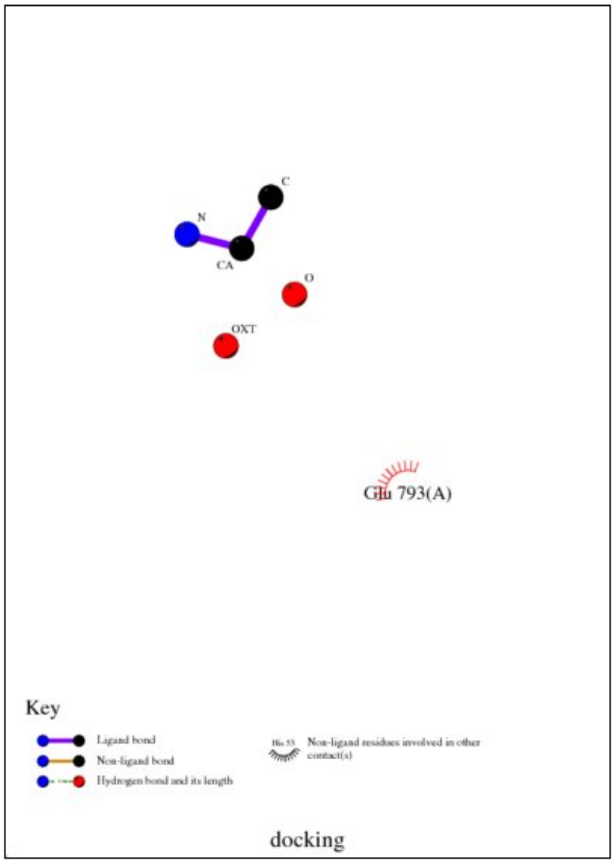

Fig. 7: The 2D plot of interaction between AMX with receptor prostate cancer mutant 2q7k–hormone.

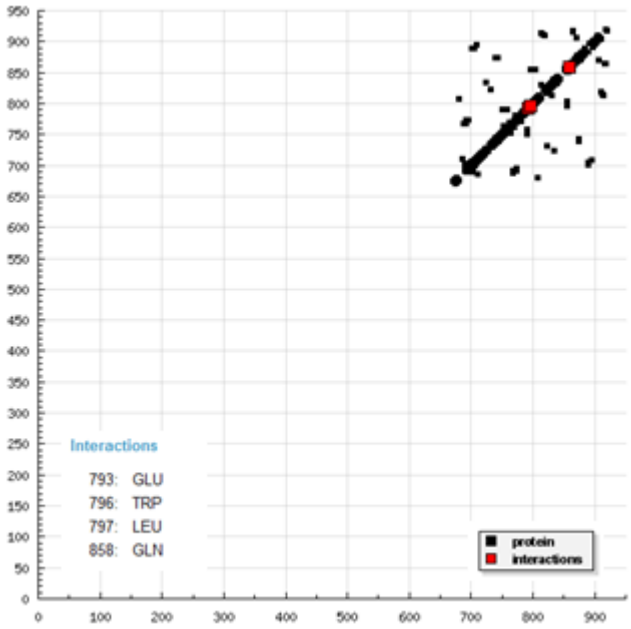

Fig. 8: HB plot of interaction between AMX drug and 2q7k receptor mutant.

References

1. M. Kubiak, A.M. Duda, M.L. Ganadu, H. Kozlowski, J. Chem. Soc. Dalton Trans.(1996)1905.
2. B. Umadevi, P.T. Muthiah, X. Shui, D.S. Eggleston, Inorg. Chim. Acta.234 (1995) 149.
3. R.A. Sanchez-del Grado, M. Navarro, H. Perez, J.A. Urbina, J. Med. Chem. 39 (1996) 1095.
4. N.B. Behrens, G.M. Diaz, D.M.L. Goodgame, Inorg. Chim. Acta.125(1986) 21.
5. J. Zhou, L.-F. Wang, J.-Y. Wang, N. Tang, J. Inorg. Biochem.83(1) (2001) 41.
6. I. Kostova, I. Manolov, I. Nicolova, S. Konstantinov, M. Karaivanova, Eur. J. Med. Chem.36(4)(2001) 339.
7. L. Ming, Med. Res. Rev. 23(2003) 697.
8. I. Turel, Coord. Chem Rev. 232(2002) 27.
9. P. Drevenski, A. Golobic, I. Turel, N. Poklar, K. Sepcic, Acta Chim. Slov. 49 (2002) 857.
10. D.E. King, R. Malone, S.H. Lilley, Am. Fam. Physicians.61(2000) 2741.
11. R.S. Srivastava, Inorg. Chim. Acta.55 (1981) L71.
12. P. Kopf-Maier, Eur. J. Clin. Pharmacol.47(1994) 1.
13. S Kalita, RK andimalla, KK Sharma, AC Kataki, M Deka, J Kotoky, Materials Science and Engineering: C., 61(2016)720-727.
14. KAM Attia, MWI Nassar, M B El-Zeiny, A Serag, Spectrochimica Acta Part A: Molecular and Biomolecular Spectroscopy, 156 (5) (2016)54-62.
15. I.P. Michael, "The Chemistry of β-Lactams". Glasgow. UK: Chapman &Hall; (1992).
16. M.A. Zayed, S.M. Abdallah, Spectrochim Acta A. 61(2005)2231.
17. M.O. Boles, R.J. Girven, P.A.C. Gane, Acta Crystallogr. B34 (1976) 461.
18. M.Castanheira, H. Sader, S. Desphande, M. Lalitagauri, R. Thomas, R.N. Jones, Antimicrobial Agents and Chemotherapy.52(2) (2008) 570.
19. S. Subramanian, C.L. Roberts, C.H. Anthony; M.H. Martin, W.S. Edwards, M.J. Rhodes, B. Campbell, J. Antimicrobial Agents and Chemotherapy.52(2) (2009) 427.
20. M.J. Neal, Medical Pharmacology at a Glance, 2nd Ed, Blackwell, Oxford (1991)78.
21. M. Neuman, Vademecum Degli Antibiotici ed Agenti Chemioterapici Anti-Infettivi, 5th Ed. (in Italian), Sigma-Tau, Rome (1994) 133.
22. D.M. Campoli-Richards, R.N. Brogden, Drugs. 33 (1987) 577.
23. W.M. Cort, J.W. Scott, M. Araujo, W.J. Mergens, M.A. Cannalonga, M. Osadca, H. Harley, D.R. Parrish, W.R. Pool, J. Am. Oil Chemists Soc.52 (1975) 174.
24. L. Seunjae, M. Yoshiki,M. Masashi, O. Hiroshi, I. Kuniyo, J. Biochem. 139 (2006) 1007.
25. M.S. Bhatia, S.G. Kashedikar, S.C. Chaturvedi, Ind Drugs.33 (1996) 213.
26. R.S. Satoskazr, S.D. Bhandarkar. Pharmacology and Pharmaco therapeutics., II, 11th Ed., Popular Prakashan., Bombay (1990) 549.
27. H.P. Rang. Pharmacology, 3rd Ed., Churchil Livinston Pub., London (1996) 691.
28. M.M. Dalc. Pharmacology, 3rd Ed., Churchil Livinston Pub., London (1998) 725.

29. P.C. Fleming, M. Goldner, D.G. Glass, Inhibition of aerobacter cephalosporin b-lactamase by penicillins. J. Bacteriol. 98 (1969) 394.
30. M. Baczkowicz, D. Wojtowicz, J.W. Anderegg, C.H. Schilling, P. Tomasik. Carbohydr. Polym.52 (2003) 263.
31. J. Delgado and W.A. Remers, "Textbook of Organic Medicinal and Pharmaceutical Chemistry", 9th ed., J. Lippincott Co. (1991) 244.
32. S.L. Lyle, S.S. Yassin, Analytica. Chim. Acta. 274(2) (1993) 225.
33. L. Pellerito, F. Maggio, M. Consiglio, A. Pellerito, G.C. Stocco, S. Grimaudo, App. Organomet. Chem. 9(3) (1995) 227.
34. R.D. Stefano, M. Scopelliti, C. Pellerito, T. Fiore, R. Vitturi, M.S. Colomba, P. Gianguzza, G.C. Stocco, M. Consiglio, L. Pellerito, J. Inorg. Biochem. 89(3–4) (2002) 279.
35. M. Imran, J. Iqbal, T. Mehmood, S. Latif, J. Biological Sciences. 6(5) (2006) 946.
36. K.I. Khallowa, N.A. Al-Omari, Tikrit J. Pure Science. 13(1) (2008) 152.
37. K. Kumar, P. Mishra, Main Group Chemistry.7(1) (2008) 1.
38. P. Mishra, Biocoordination Int. J. Pharma. Sci. Rev. Research.3(2)(2010) 28.
39. S. Joshi, V. Pawar, V. Uma, Int. J. Pharma. Bio. Sci. 2(1) (2011) 32.
40. V.G. Alekseev, V.G. Zamyslov, Russ. J. Coord. Chem. 33(4) (2007) 254.
41. D.Arefi, F.Maknoni, R.S. Khoshnood, Clinical Biochemistry. 44 (13)(2011) S265.
42. N.M. El-Metwaly, M.S. Refat, Spectrochim. Acta Part A.78 (2011) 196.
43. M.S. Refat, S.F. Mohamed, Spectrochim. Acta A.82 (2011) 108.
44. M.S. Refat, J. Mol. Str. 1037 (2013) 170.
45. M.S. Refat, Spectrochim. Acta Par A. 105 (2013) 326.
46. S.M. El-Megharbel, R.Z. Hamza, M.S. Refat, Spectrochim. Acta Part A. 131C (2014) 534.
47. S.M.El-Megharbel, R.Z. Hamza, M.S. Refat, Chemico-Biological Interactions. 220 (2014) 169.
48. M.S. Refat, Spectrochimica Acta Part A.68 (2007) 1393.
49. K. Nakamoto Infrared and Raman spectra of inorganic and coordination compound. New York: Wiley (1978).
50. N. Kanooco, R.V. Singh, J.P. Tandon, Syn. React. Inorg. Met. Org. Chem.17 (1987) 837.
51. G.B. Deacon, R. J. Phillips, Coord. Chem. Rev. 33(1980) 227.
52. J.R. Anacona, E.M. Figueron, J. Coord. Chem.48 (1999) 181.
53. O.F. Ozturk, M. Sekerci, E. Ozdemir, Russ. J. Coord. Chem. 31 (2005) 687.
54. O.F. Ozturk, M. Sekerci, E. Ozdemir, Russ J Gen Chem.76 (2006) 33.
55. B.N. Figgis, "Introduction to Ligand Fields",Interscience Publishers, John Wiley and Sons, New York. (1967) 285.
56. B.J. Hathaway, D.E. Billing, Coord. Chem. Rev. 5 (1970) 143
57. B.J. Hathaway, Struct. Bonding (Berlin) 57 (1984) 55.
58. C.J. Carrano, C.M. Nunn, R. Quan, J.A. Bonadies, V.L. Pecoraro, Inorg. Chem. 29 (1990) 944.
59. N.K. Gaur, R. Sharma, R.S. Sindhu, J. Indian Chem. Soc. 78 (2001) 26.
60. B.G. Kalagouda, A.P. Siddappa, S.V. Rashmi, S.P. Manjula, J. Serb. Chem. Soc.71(5) (2006) 529.
61. T.M. Ismail. J. Coord. Chem. 58 (2005) 141.
62. A.B.P. Lever. J. Chem. Edu.45 (1968) 711.
63. B. Adhikari, S. Liu and C.R. Lucas. Inorg. Chem.32 (1993) 5957.

64. Z.H. Abd El-Wahab, Spectrochim. Acta A. 67 (2007) 25.
65. A. W. Coats, J. P. Redfern, Nature . 201 (1964) 68.
66. H.W. Horowitz, G. Metzger, G., Anal. Chem. 35 (1963) 1464.
67. K. K. M. Yusuff, R. Sreekala, Thermochim Acta.159 (1990) 357.
68. A. A. Frost, R. G. Peasron, "Kinetics and Mechanism", Wiley, New York, (1961).
69. G.M. Morris, D.S. Goodsell, J. Comput. Chem. 19 (1998) 1639.
70. A.Z. El-Sonbati, G.G. Mohamed, A.A. El-Bindary, W.M.I. Hassan, M.A. Diab, Sh.M. Morgan, A.K. Elkholy, J. Mol. Liq. 212 (2015) 487.
71. A. Halgren, J. Computat. Chem. 17 (1998) 490.

Highlights

- Preparation of of Cu(II), Co(II), Ni(II) and Fe(III) chelates of amoxicillin antibiotic drug.
- Spectroscopic and thermal analyses were performed.
- The stoichiometry of 1:2 (Metal : AMX) complexes was explained .
- The values of molar conductance for the AMX complexes led to electrolytic behavior.